ChemPhotoChem

Supporting Information

Photophysical Properties of Indocyanine Green in the Shortwave Infrared Region

Emily D. Cosco, Irene Lim, and Ellen M. Sletten*

Table of Contents:

I. Supporting tables

Table S1. Photophysical properties of ICG from the literature

Ref.	Year	Solvent	$\lambda_{max,abs}$ (nm)	ε ($M^{-1}cm^{-1}$)	$\lambda_{max,em}$ (nm)	Φ_F (%)
1	2011	EtOH	787	194,000 ± 6,000	818	13.2 ± 0.8
2	2002	EtOH	780	130,000	830	n.r.
3	1994	EtOH	786	194,400	n.r.	5 ± 1
4	2015	MeOH	785	204,000	822	7.8
5	2014	MeOH	785	n.r.	814	7.2
6	1996	MeOH	785	248,000	822	4.1 ± 0.6
7	1996	MeOH	782	n.r.	n.r.	4.3 ± 0.5
3	1994	MeOH	782	195,300	n.r.	4.0 ± 0.8
8	1978	MeOH	n.r.	n.r.	820	8 ± 2
9	2020	DMSO	n.r	n.r.	n.r.	26.2
10	2012	DMSO	n.r.	n.r.	n.r.	22.8 ± 0.7
8	1978	DMSO	n.r.	n.r.	835	12 ± 2
11	1977	DMSO	795	n.r.	835	13
9	2020	Water	n.r.	n.r.	n.r.	3.7
12	2018	Water	n.r.	150,000	n.r.	0.9
13	2016	Water	779	n.r.	805	2.4 ± 0.2
6	1996	Water	779	175,000	810	1.2 ± 0.2
7	1996	Water	780	n.r.	n.r.	2.7 ± 0.5
3	1994	Water	779	n.r.	n.r.	1.0 ± 0.2
8	1978	Water	n.r.	n.r.	820	0.28 ± 0.06
14	2010	70:30 EtOH:water	n.r.	n.r.	n.r.	8.4 ± 0.1
15	2019	PBS	779	111,060	807	1.7
10**Error! Bookmark not defined.**	2012	PBS	n.r.	n.r.	n.r.	2.7 ± 0.2
14	2010	PBS	780	n.r.	n.r.	2.7 ± 0.1

16	2010	PBS	780	n.r.	810	4
17	2005	PBS	779	110,000	806	1
18	2000	PBS	780	115,000	812	1.2
6	1996	PBS	780	115,000	812	1.3 ± 0.2
17	2005	FBS	800	166,000	811	9
18	2000	bovine plasma	803	215,000	830	3.2
6	1996	plasma	803	215,000	829	~4 ± 1
7	1996	HSA[a]	800	n.r.	n.r.	4.0 ± 0.5
16	2010	BSA[b]	807	n.r.	822	8
8	1978	whole blood	n.r.	n.r.	830	1.2 ± 0.2

[a]HSA was prepared at 50 g/dm^3 in Hydrion pH 7.4 buffer. [b]BSA was prepared as 5 mass% (w/v) BSA in PBS.

II. Supporting Figures

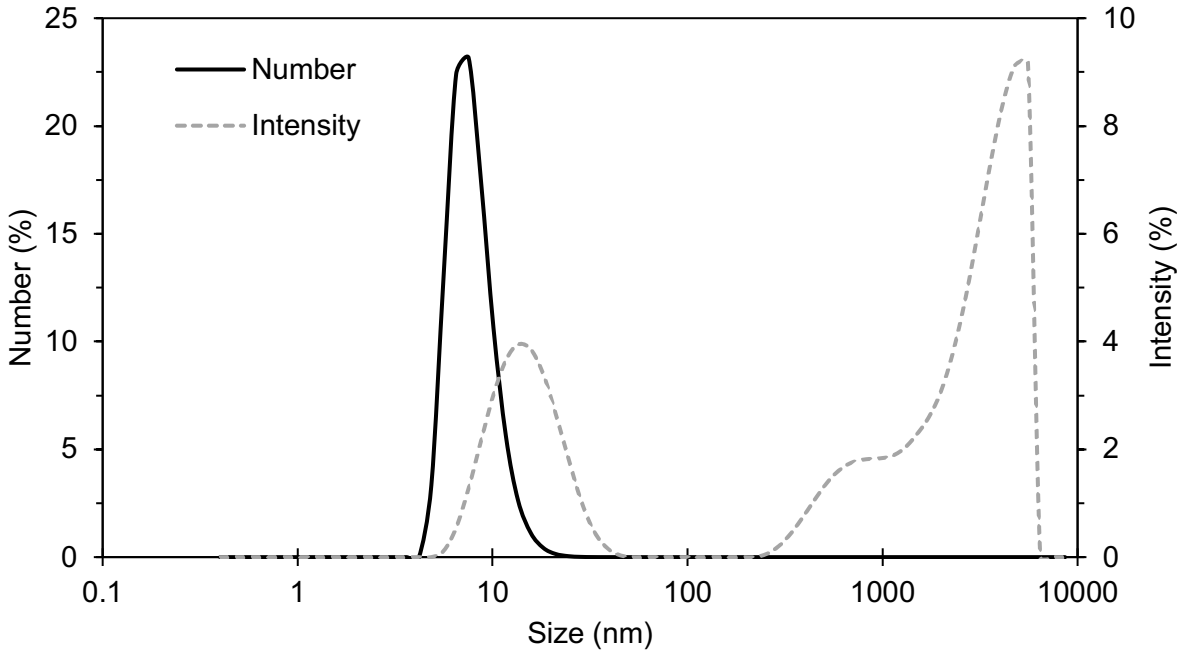

Figure S1. Dynamic light scattering (DLS) characterization of PEG-phospholipid micelles containing ICG, composed of 18:0 PEG2000 PE lipids. Number and intensity plots are provided as the solid (black) and dashed (gray) lines, respectively. The number average is 8.0 ± 0.2 nm. The intensity average is 14 ± 5 nm. Larger populations are also present at 589 nm and 4348 nm, representing 17.2%, and 53.4% in total intensity, respectively. As intensity is proportional to diameter to the sixth power, the observed aggregation is a minimal percentage of the total species (~1 x 10^{-8} %). Data are the average of three measurements, error represents the standard deviation.

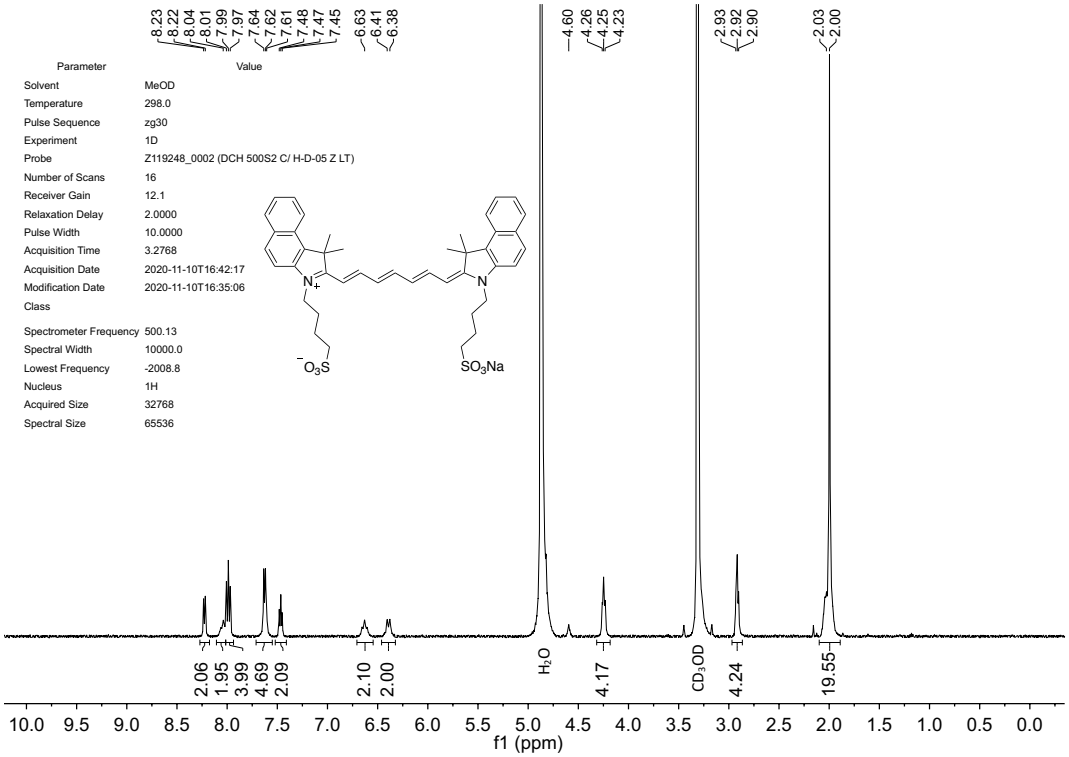

Figure S2. ^{1}H NMR of ICG in MeOD. Spectrum is in agreement with the literature.[19]

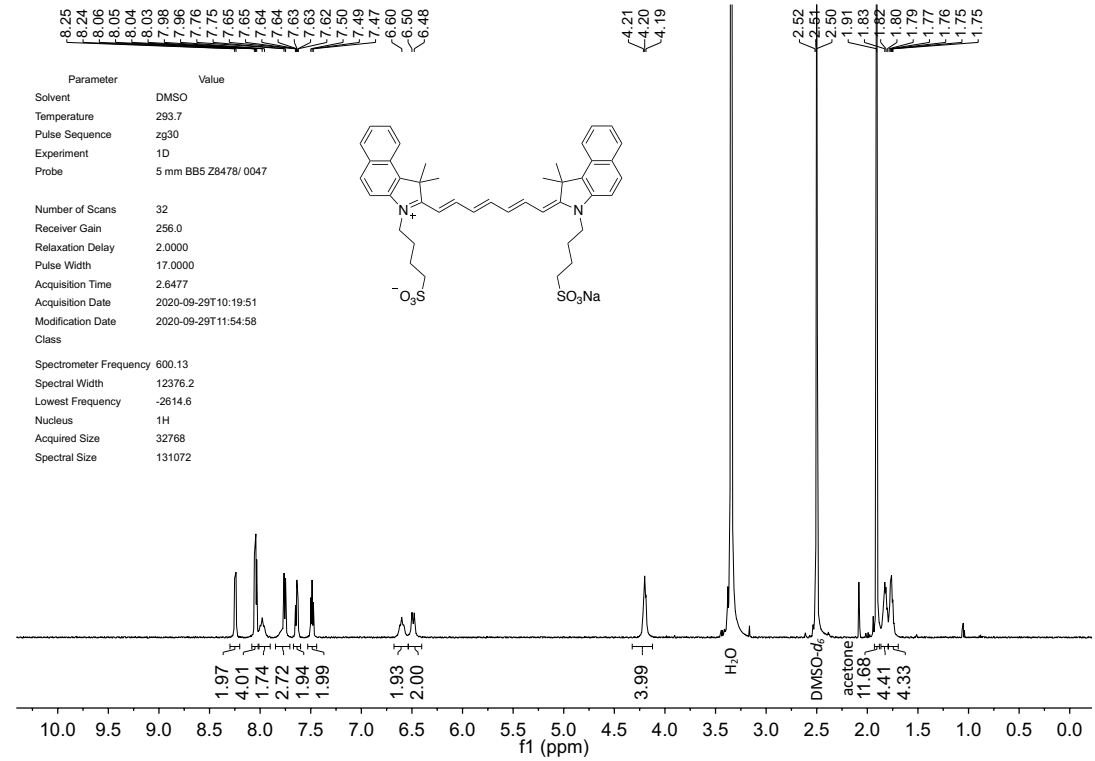

Figure S3. ^{1}H NMR of ICG in DMSO-d_6.

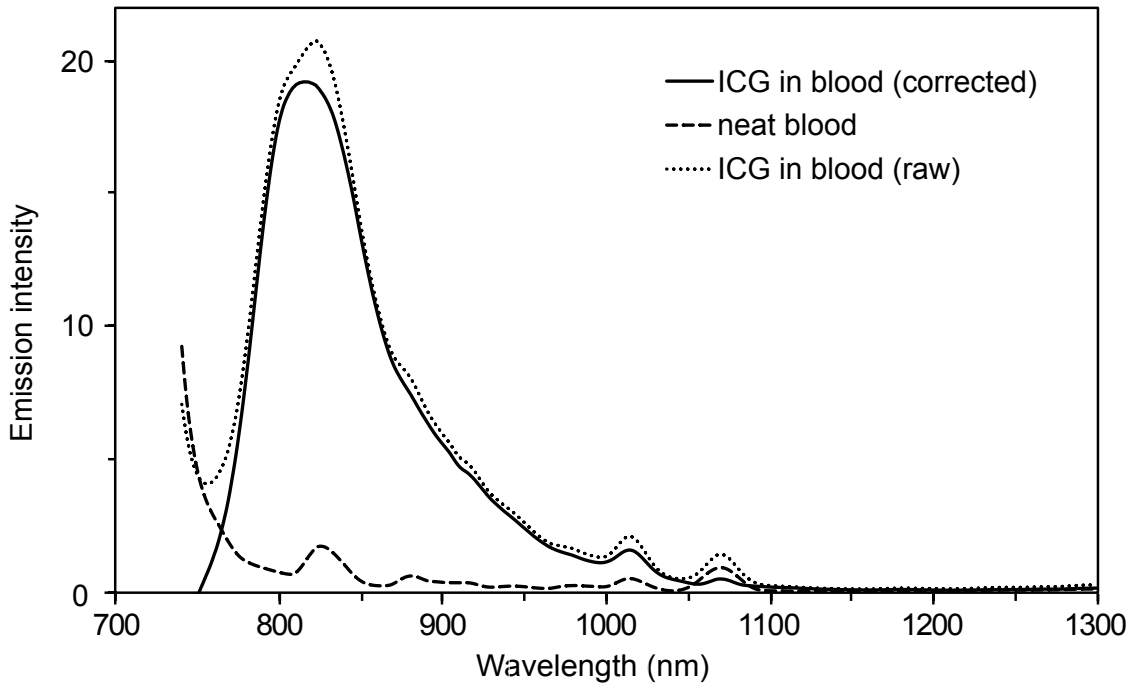

Figure S4. Correction for emission trace of ICG in blood (excitation wavelength = 710 nm). The emission of neat blood (dashed) is subtracted from the raw ICG in blood trace (dotted) to produce the corrected emission trace (solid).

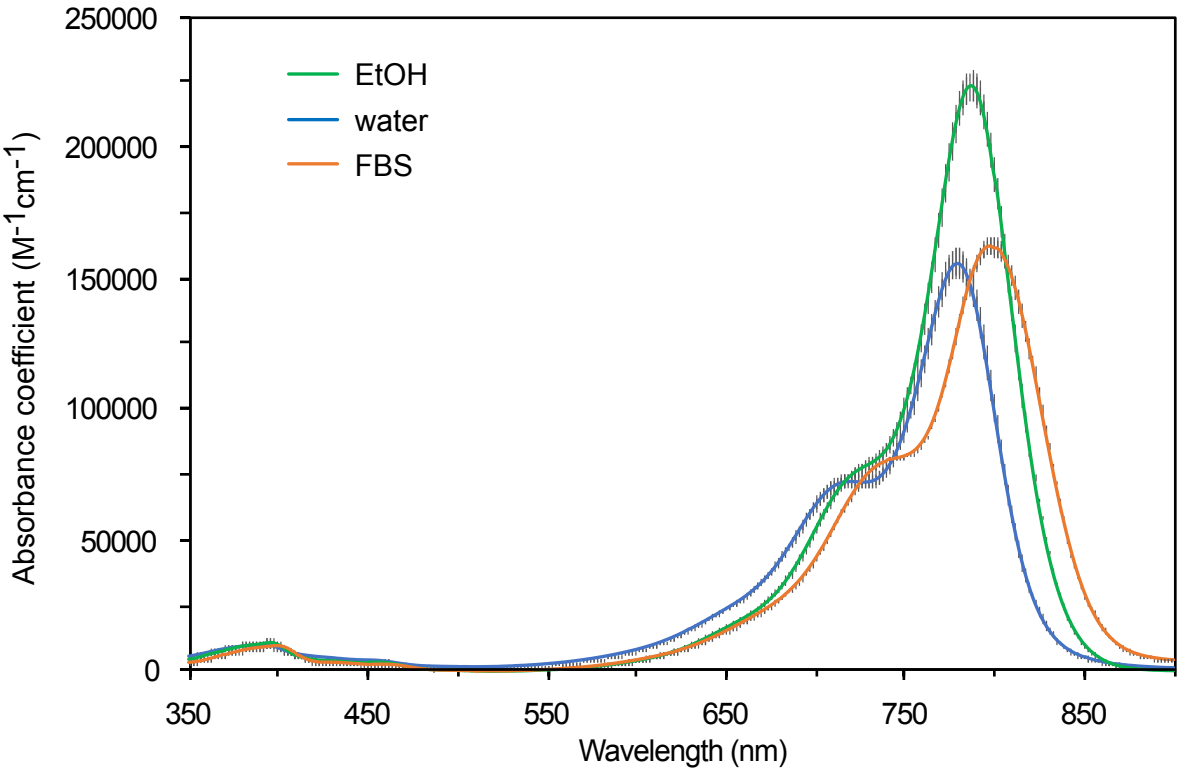

Figure S5. Absorption coefficient traces of ICG in water (blue), absolute ethanol (green), and fetal bovine serum (orange). Error bars are the standard deviation of three measurements.

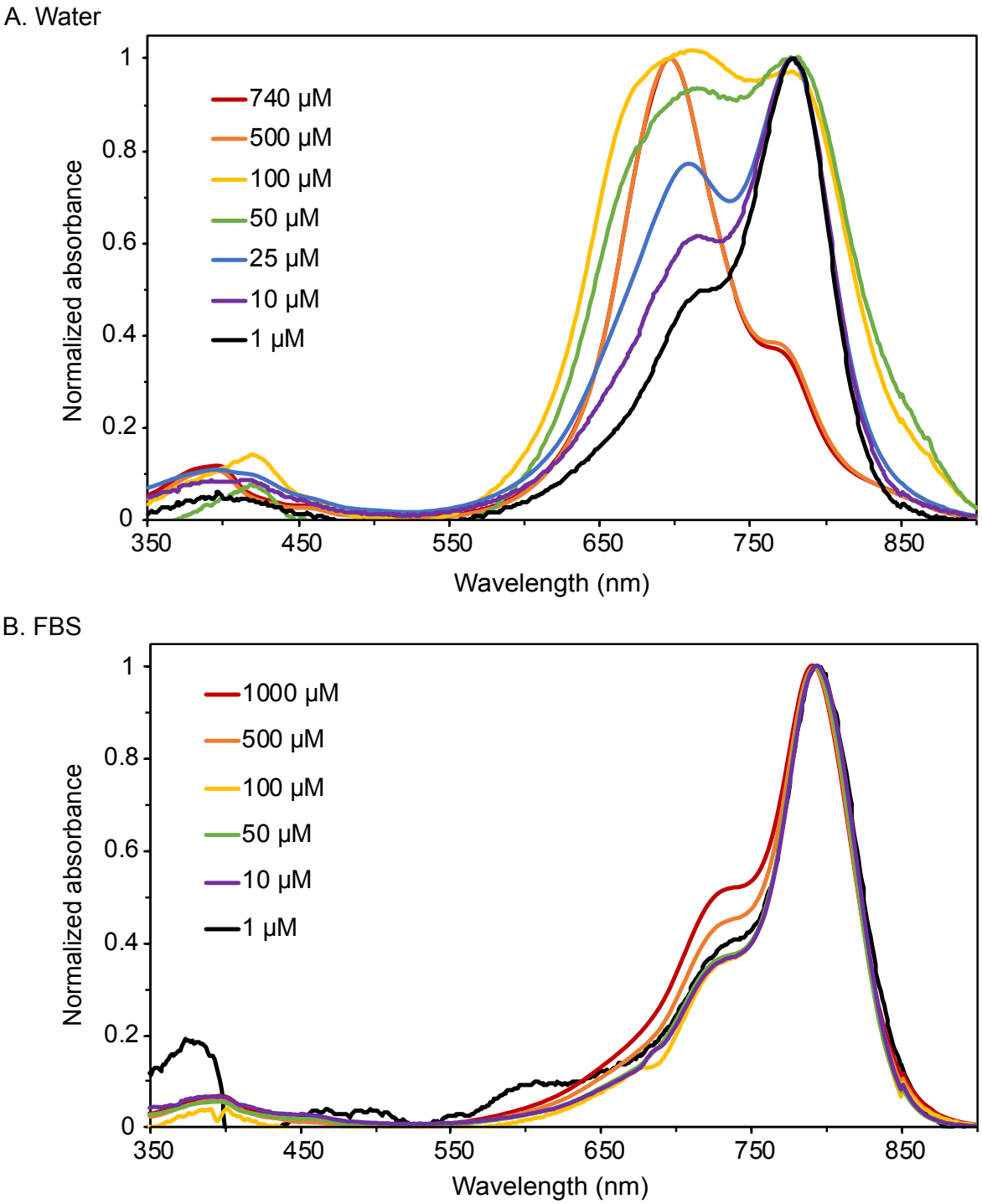

Figure S6. Absorbance traces of ICG in water (A) and FBS (B) at varying concentrations, from 1 μM to 1 mM.

A.

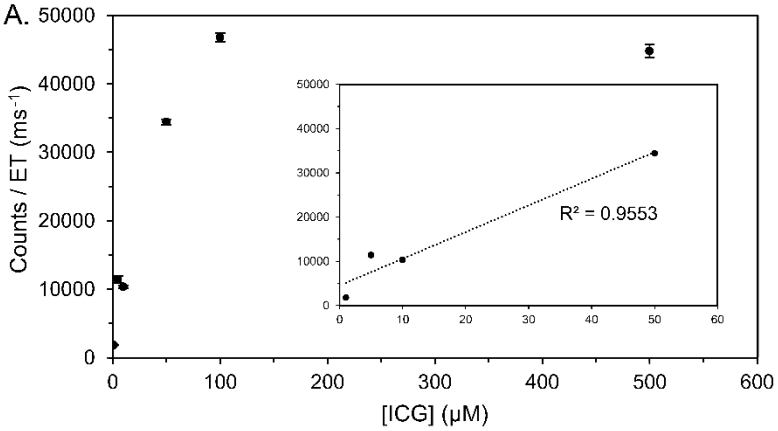

B.

[ICG] (μM)	Counts/ET (ms^{-1})
1	1820 ± 20
5	11500 ± 500
10	10300 ± 200
50	34400 ± 400
100	46800 ± 600
500	46000 ± 1000

Figure S7. Linearity of ICG signal to concentration in SWIR imaging configuration. A) Brightness of capillaries containing different concentrations of ICG in ethanol (1, 5, 10, 50, 100, 500 μM). Inset displays the linear range of detection on the InGaAs detector from 1 to 50 μM (R^2 = 0.95). Error is the standard deviation of three replicates. B) Table displaying ICG concentration and counts with error. Error represents the standard deviation of 3 replicate measurements.

Note: In clinical studies, ICG dosages range from 0.5 mg/kg[23] to 10 mg/kg.[24] Assuming a body weight of 20 g and a blood volume of 2 mL in mice, these dosages convert to roughly 6 μM to 130 μM. Since this range is partially within the region of linearity for the InGaAs detection system used here, caution should be used when drawing quantitative conclusions.

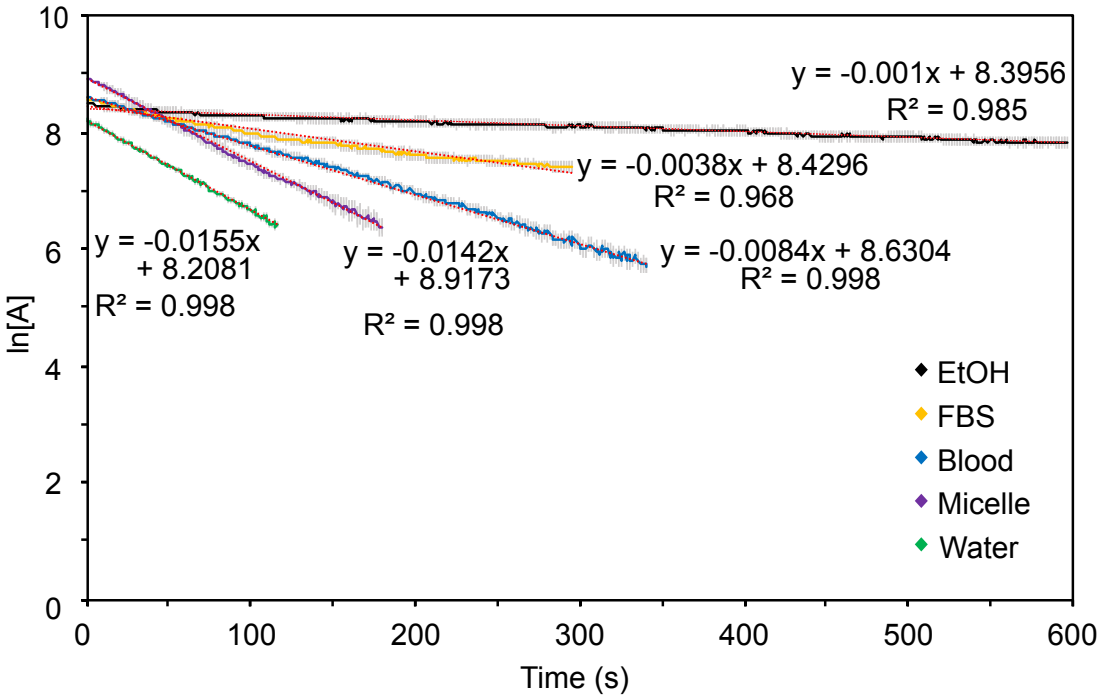

Figure S8. Photobleaching data plotted as the ln[A] vs. time and the corresponding linear fits. ICG was dissolved in each medium (absolute ethanol, black; FBS, yellow; blood, blue; micelle formulation, purple; and milliQ water, green) at 5 μM. The decrease in emission is depicted on a logarithmic scale. Error bars are the standard deviations of 3 replicate measurements.

Note: As all photobleaching experiments were performed with the same laser wavelength and irradiation, and the absorption maxima of ICG changes only slightly in the solvents studied, photobleaching rates are reported as raw rates without any corrections for wavelength, power density, or the number of absorbed photons. The raw rates most closely represent the effects one would observe in an imaging experiment.

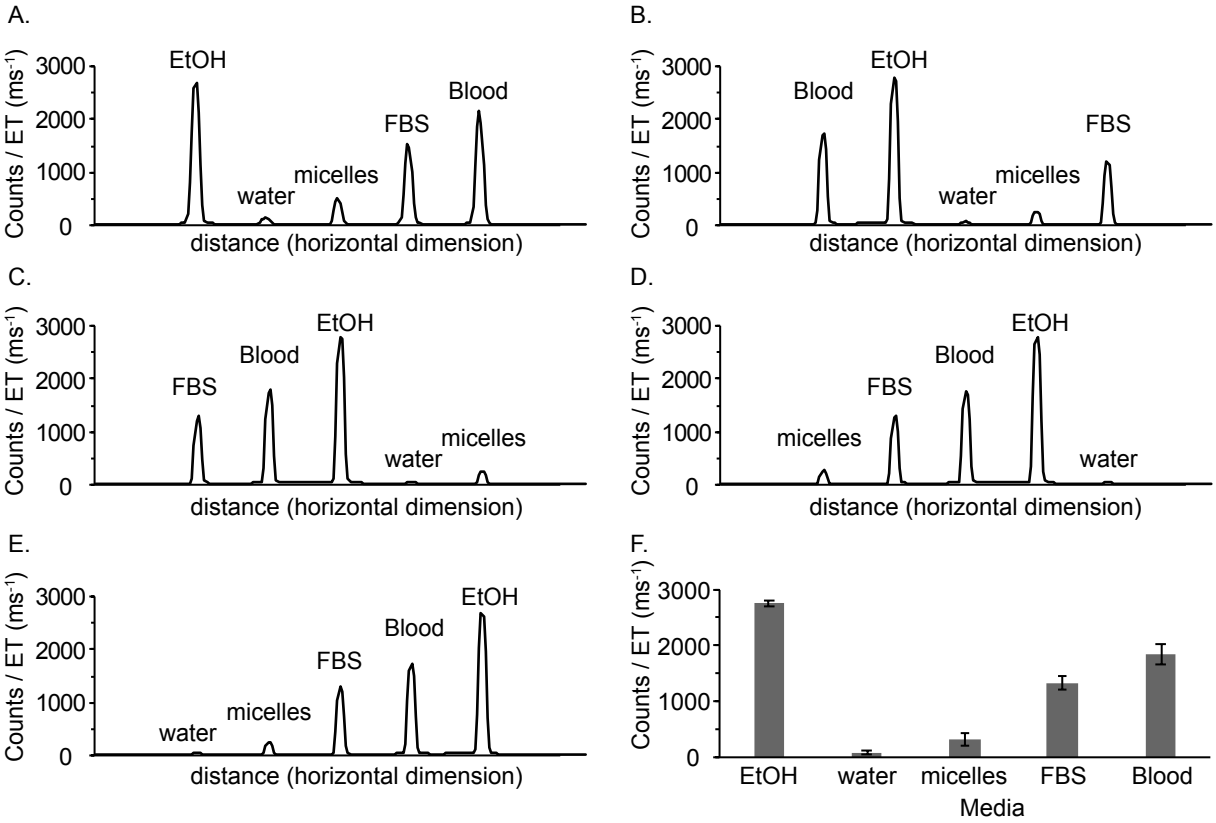

Figure S9. Brightness of capillaries containing equal concentrations (5 μM) of ICG in several solvents, positioned over five imaging locations (A–E) and compiled (F). Capillaries were excited with an average laser irradiation of 63 $mWcm^{-2}$ and collected with 1,100 nm longpass filtering and an exposure time of 5 ms. Error in (F) is the standard deviation of the five measurements.

III. Abbreviations

BSA, bovine serum albumin; DLS, dynamic light scattering; DMSO, dimethylsulfoxide; EtOH, ethanol; FBS, fetal bovine serum; fps, frames per second; HSA, human serum albumin; ICG, indocyanine green; IDE, integrated development environment; LP, longpass; MeOH, methanol; MeOD, methanol-d_4; NIR, near-infrared; PBS, phosphate buffered saline; PEG, poly(ethylene glycol); SOP, standard operating procedure; UV, ultra violet; VIS, visible.

IV. References

[1] K. Rurack, M. Spieles, *Anal. Chem.* **2011**, *83*, 1232–1242.
[2] K. Kassab, *J. Photochem. Photobiol. B Biol.* **2002**, *68*, 15–22.
[3] S. A. Soper, Q. L. Mattingly, *J. Am. Chem. Soc.* **1994**, *116*, 3744–3752.
[4] R. R. Nani, J. B. Shaum, A. P. Gorka, M. J. Schnermann, *Org. Lett.* **2015**, *17*, 302–305.
[5] O. A. Okoh, R. H. Bisby, C. L. Lawrence, C. E. Rolph, R. B. Smith, *J. Sulfur Chem.* **2014**, *35*, 42–56.
[6] K. Licha, B. Riefke, W. Semmler, in *Proc. SPIE* **1996**, *2927*, 192–198.
[7] R. Philip, A. Penzkofer, W. Baumler, R. M. Szeimies, C. Abels, *J. Photochem. Photobiol. A-Chemistry* **1996**, *96*, 137–148.
[8] R. C. Benson, H. a Kues, *Phys. Med. Biol.* **1978**, *23*, 159–163.
[9] R. Hoshi, K. Suzuki, N. Hasebe, T. Yoshihara, S. Tobita, *Anal. Chem.* **2020**, *92*, 607–611.
[10] C. Würth, J. Pauli, C. Lochmann, M. Spieles, U. Resch-Genger, *Anal. Chem.* **2012**, *84*, 1345–1352.
[11] R. C. Benson, H. A. Kues, *J. Chem. Eng. Data* **1977**, *22*, 379–383.
[12] J. A. Carr, D. Franke, J. R. Caram, C. F. Perkinson, M. Saif, V. Askoxylakis, M. Datta, D. Fukumura, R. K. Jain, M. G. Bawendi, O. T. Bruns, *Proc. Natl. Acad. Sci.* **2018**, *115*, 4465–4470.
[13] T. Jin, S. Tsuboi, A. Komatsuzaki, Y. Imamura, Y. Muranaka, T. Sakata, H. Yasuda, *Med. Chem. Commun.* **2016**, *7*, 623–631.
[14] T. J. Russin, E. Ï. Altmoğlu, J. H. Adair, P. C. Eklund, *J. Phys. Condens. Matter* **2010**, *22*, 334217.
[15] S. Thavornpradit, S. M. Usama, G. K. Park, J. P. Shrestha, S. Nomura, Y. Baek, H. S. Choi, K. Burgess, *Theranostics* **2019**, *9*, 2856–2867.
[16] J. Pauli, R. Brehm, M. Spieles, W. A. Kaiser, I. Hilger, U. Resch-Genger, *J. Fluoresc.* **2010**, *20*, 681–693.
[17] S. Obnisbi, S. J. Lomnes, R. G. Laurence, A. Gogbasbian, G. Mariant, J. V. Frangioni, *Mol. Imaging* **2005**, *4*, 172–181.
[18] K. Licha, B. Riefke, V. Ntziachristos, A. Becker, B. Chance, W. Semmler, *Photochem. Photobiol.* **2000**, *72*, 392.
[19] F. Rüttger, S. Mindt, C. Golz, M. Alcarazo, M. John, *European J. Org. Chem.* **2019**, *2019*, 4791–4796.